

Al-clad Cu bond wires for power electronics packaging

Microstructure evolution, mechanical performance, and molecular dynamics simulation of diffusion behaviors

Liu, Wenting; Wang, Xinyue; Zhang, Jing; Zhang, Guoqi; Liu, Pan

DOI

[10.1016/j.mtcomm.2024.110940](https://doi.org/10.1016/j.mtcomm.2024.110940)

Publication date

2024

Document Version

Final published version

Published in

Materials Today Communications

Citation (APA)

Liu, W., Wang, X., Zhang, J., Zhang, G., & Liu, P. (2024). Al-clad Cu bond wires for power electronics packaging: Microstructure evolution, mechanical performance, and molecular dynamics simulation of diffusion behaviors. *Materials Today Communications*, 41, Article 110940. <https://doi.org/10.1016/j.mtcomm.2024.110940>

Important note

To cite this publication, please use the final published version (if applicable). Please check the document version above.

Copyright

Other than for strictly personal use, it is not permitted to download, forward or distribute the text or part of it, without the consent of the author(s) and/or copyright holder(s), unless the work is under an open content license such as Creative Commons.

Takedown policy

Please contact us and provide details if you believe this document breaches copyrights. We will remove access to the work immediately and investigate your claim.



Al-clad Cu bond wires for power electronics packaging: Microstructure evolution, mechanical performance, and molecular dynamics simulation of diffusion behaviors

Wenting Liu^a, Xinyue Wang^a, Jing Zhang^b, Guoqi Zhang^c, Pan Liu^{a,d,*}

^a Academy for Engineering & Technology, Fudan University, Shanghai 200433, China

^b Heraeus Materials Technology Shanghai Ltd., Shanghai 201108, China

^c Department of Microelectronics, Delft University of Technology, Delft 2628 CD, the Netherlands

^d Research Institute of Fudan University in Ningbo, Zhejiang 315336, China

ARTICLE INFO

Keywords:

Wedge bonding
Heat treatment
Intermetallics
Mechanical properties
Molecular dynamics

ABSTRACT

With the advancement of power electronics, aluminum-clad copper thick bonding wires have garnered attentions due to superior electrical and thermal properties, making them well-suited for high-temperature and high-current applications. However, the impact remains unveiled of whether the growth of intermetallic compounds (IMCs) at the bonding interface presents critical challenges to the reliability of wedge wire bonds. Therefore, it is necessary to investigate the evolution behavior of Cu/Al IMCs in Al-clad copper wires. In this study, Scanning Electron Microscopy (SEM) and Transmission Electron Microscopy (TEM) were firstly employed to characterize the phase composition and growth behavior of Cu/Al intermetallic compounds (IMCs) at two distinct interfaces—the bonding interface and the core-shell interface—under various annealing conditions during high-temperature storage (HTS) tests, revealing a parabolic relationship between aging time and IMCs thickness. Subsequently, shear and pull tests of Al-clad copper bond wires were conducted to evaluate the bonding strength under different aging conditions, clarifying the correlation between various failure modes of the bonds and the evolution of IMCs at the bi-interfaces of this novel composite across different aging stages. Additionally, molecular dynamics (MD) simulations were employed to explore the diffusion behavior of Cu and Al atoms. It revealed that polycrystalline structures enhanced the mutual diffusion at the interface, with copper serving as the predominant element in the interdiffusion process. In conclusion, this study integrates experimental and numerical approaches to elucidate the growth mechanisms of Cu/Al intermetallic compounds and their effects on reliability, providing valuable guidance for optimizing the performance of composite bonding wires in high-temperature power device applications.

1. Introduction

The rapid development of the power electronics industry has placed increasing demands on power semiconductor devices, particularly regarding their ability to operate effectively under high temperatures and high currents, thereby challenging the reliability of electronic packaging[1–5]. Wire bonding, as the conventional technology for chip interconnection, has encountered limitations[6,7]. With traditional aluminum (Al) thick wires used in ultrasonic wedge bonding for power electronics, failures often occur due to the low melting point and inadequate mechanical properties[8,9]. In recent years, aluminum-clad copper bond wires have emerged as a promising alternative,

exhibiting enhanced mechanical, electrical, and fatigue properties under demanding conditions[10–13]. However, the influence of intermetallic compounds (IMCs) formed at the copper/aluminum (Cu/Al) interface remains unclear under high-temperature conditions, particularly with respect to Al-clad Cu bonds that exhibit two distinct interfaces: the bonding interface and the core-shell interface. Therefore, it is essential to investigate the growth and evolutionary behaviors of IMCs at the bi-interfaces of these novel composite bonds during high-temperature storage tests.

To date, various Cu/Al intermetallic compounds form at high temperatures, including CuAl₂, CuAl, Cu₃Al₂, Cu₄Al₃, and Cu₉Al₄[14–16]. Most documented studies have focused on the interfaces of ball bonds of

* Corresponding author at: Academy for Engineering & Technology, Fudan University, Shanghai 200433, China.

E-mail address: panliu@fudan.edu.cn (P. Liu).

<https://doi.org/10.1016/j.mtcomm.2024.110940>

Received 2 April 2024; Received in revised form 19 October 2024; Accepted 8 November 2024

Available online 9 November 2024

2352-4928/© 2024 The Authors. Published by Elsevier Ltd. This is an open access article under the CC BY license (<http://creativecommons.org/licenses/by/4.0/>).

thin Cu wire bonds on Al substrates[17–21]. Xu et al. observed that CuAl_2 formed initially at lower temperatures, followed by Cu_9Al_4 as temperatures increased [19]. This sequence of intermetallic compounds formation was driven by both thermodynamic and kinetic factors. Numerous work have focused on the mechanical properties of Cu/Al IMCs. Their findings indicate that copper-rich phases, such as Cu_9Al_4 , exhibited superior mechanical strength compared to aluminum-rich phases[18,20]. Additionally, it is important to note that excessive IMC thickness is considered unacceptable due to its intrinsic brittleness and the potential for Kirkendall void formation, which significantly reduces the mechanical strength[22–24]. Moreover, the exploration of mutual diffusion behaviors has been conducted through molecular dynamics (MD) simulations at the atomic level [25–28]. These simulations revealed that temperature was a crucial parameter significantly influencing the Cu/Al mutual diffusion process.

However, wedge bonds utilizing thick wires exhibit distinct characteristics that differ significantly from ball bonds, including preferences for wire diameter and bond deformation profiles. These variations profoundly affect the contact area at the interface of dissimilar metals, thereby influencing the formation and growth of interfacial intermetallic compounds. Furthermore, existing simulations predominantly focus on diffusion processes within monocrystalline materials, which does not accurately represent the typical polycrystalline nature of the actual bond wire materials. Additionally, the mutual diffusion mechanism in the Cu/Al system—particularly the relationship between Cu/Al IMCs thickness and growth time—remains unvalidated through simulation studies.

Therefore, this paper aims to investigate the diffusion behaviors of the Cu/Al binary system in Al-clad copper thick wires of wedge bonds such thick Cu-Al composite bond wires, encompassing both the practical experiments and the molecular dynamic simulations. The technical roadmap of this work was presented in Fig. 1. Firstly, the Cu/Al IMCs grown at both bonding and core-shell interfaces were characterized, with an investigation of the growth mechanism. Additionally, the mechanical tests were also performed to evaluate the influences of the IMCs on the shear and pull strength of the bonds. Lastly, to further study the mechanism, molecular dynamics simulations were conducted to observe the dynamic diffusion process in polycrystalline materials and verify the

growth mechanism from the simulation perspective. This research contributes to understanding and modulating the Cu/Al IMCs growth, elucidating the relationship between the IMCs thickness and mechanical strength, thereby enhancing the reliability of bond wires for high-temperature packaging of power devices.

2. Materials and methods

2.1. Materials and bonds preparation

A commercial 300 μm diameter Al-clad copper bond wire, Cucor Al Plus, with a 1:1 vol ratio of copper to aluminum, was sourced from Heraeus. The purity of the copper core, and the aluminum shell are both 99.99 %. Then, the bond wires were bonded on the substrates purchased from Ferrotec using the Asterion™ wedge bonder supplied by K&S company.

2.2. High-temperature storage test (HTS)

High-temperature storage tests were conducted at 250 °C, 300 °C, and 350 °C with 4 varying aging times each to expedite the growth of Cu/Al intermetallic compounds. The furnace (SG-XL 1200) was applied to provide a high-temperature environment, and the aging process was carried out in the air.

2.3. Bonds mechanical tests

Shear and pull tests were performed using a shear tester (Nordson, Dage 4000) to assess the mechanical strength of the bonds. A minimum of 15 effective values for each test were recorded to calculate the average value. The shear height was 20 μm , and the shear speed was 300 $\mu\text{m/s}$.

2.4. Phase characterization

To observe the formation and growth behaviors of the Cu/Al IMCs, optical microscopy (OM, KEYENCE) and Scanning Electron Microscopy with Energy Dispersive X-ray Spectroscopy (SEM-EDS, Zeiss) were employed for initial characterization and identification of the occurring phases. Subsequently, the accurate verification of each phase was achieved using Selected Area Electron Diffraction (SAED) patterns obtained from a Transmission Electron Microscope (TEM).

2.5. Molecular dynamics simulation

2.5.1. Simulation model establishment

As shown in Fig. 2, four diffusion models with the different types of the material nature were established in ATOMSK to simulate the diffusion process. To minimize the crystal mismatch between the Cu and the Al, the upper part of the Model A comprises a supercell of the Al atoms with dimensions of $25 \times 25 \times 17 (L_{\text{Al}})^3$ and the lower part comprises a supercell of the Cu atoms with dimensions of $28 \times 28 \times 17 (L_{\text{Cu}})^3$ (L_{Al} and L_{Cu} representing the lattice constants of aluminum and copper atoms, respectively). In all constructions, the contact plane of each monocrystalline model was defined as the (001) plane. The polycrystalline models (Model B, C and D) with random grain size as well as the distribution were constructed based on Voronoi method and the number of the grains was set as 25.

2.5.2. Simulation parameters setup

The simulations were executed using the Large-scale Molecular Massively Parallel Simulator (LAMMPS) and visualized in OVITO. Initial velocities of atoms were randomly assigned following the Maxwell-Boltzmann rate distribution. The Newton equation of motion for atoms was solved using the Verlet integral method [29]. Under the NPT ensemble, the model was first relaxed in a vacuum environment at 298 K

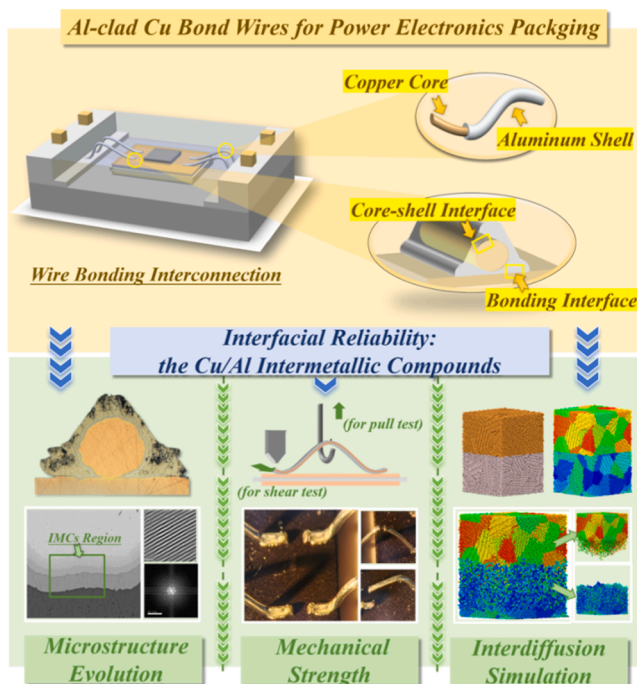


Fig. 1. The technical roadmap of this work.

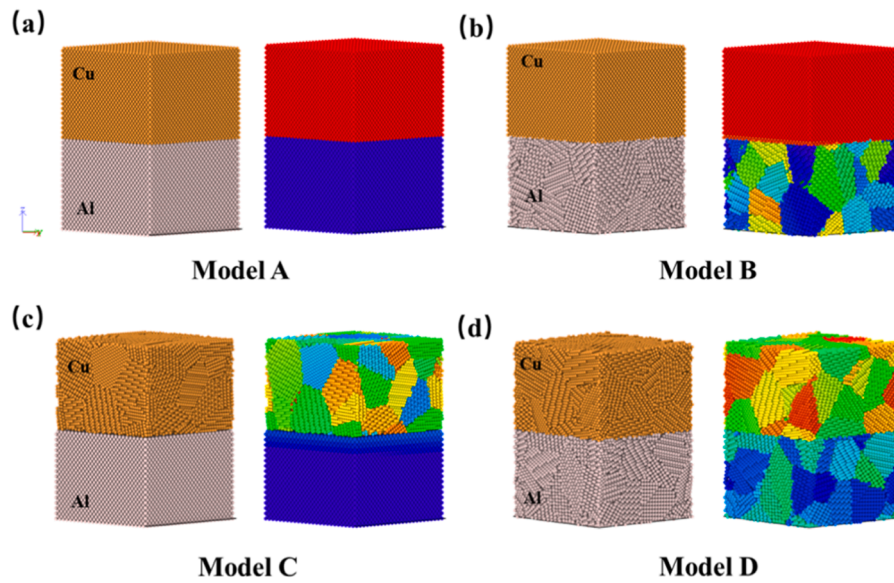


Fig. 2. The established models with various materials nature.

to reach the thermodynamic equilibrium state. Then, the temperature of the system was quickly raised to the preset temperature by the Nose-Hoover hot bath method [30] to start the simulation. The time step was set at 2 fs, with a total of 200,000 run steps. Throughout the diffusion simulation, a pressure of one atmosphere was maintained in the x and y directions. Periodic boundary conditions were applied in the x and y directions of the model. The top and bottom five layers of atoms were fixed to prevent volume changes during the simulation. The Embedded Atomic Method (EAM) function, proposed by Cai et al. [31],

was employed to describe the potential function between atoms.

3. Results and discussions

To explore the impact of IMCs on interfacial properties and elucidate the mechanism of Cu/Al mutual diffusion, comprehensive studies were undertaken and discussed across microstructure evolution, mechanical performance, and molecular dynamics simulations.

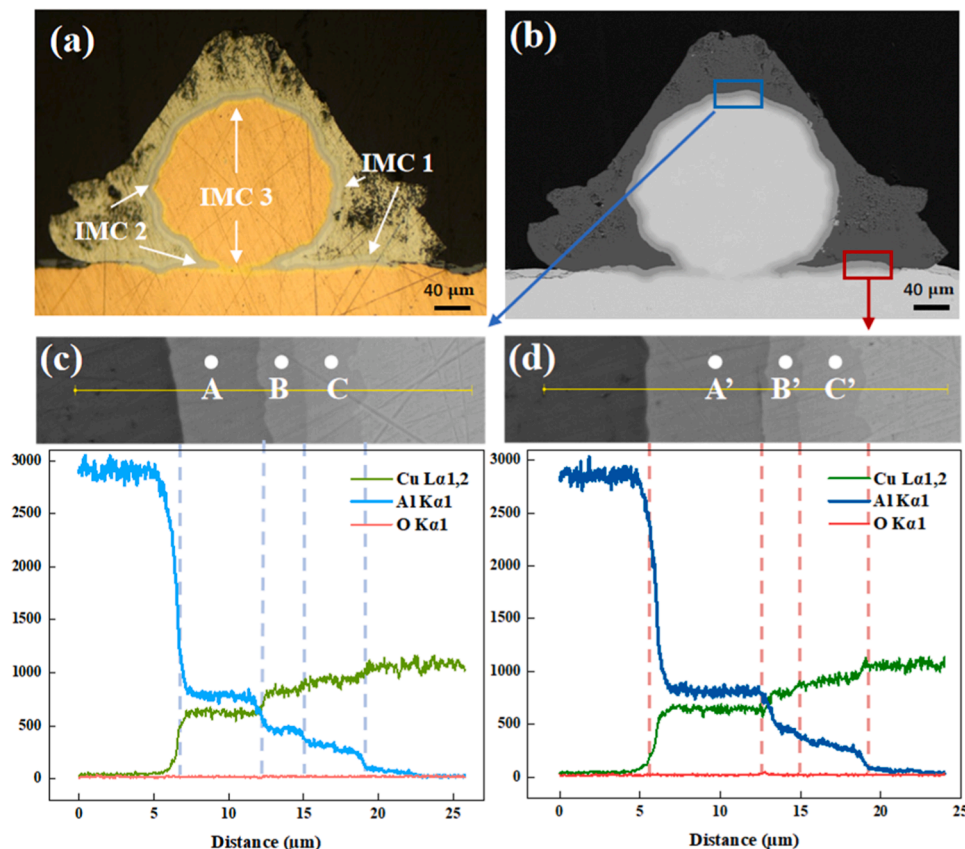


Fig. 3. The morphology characterization and composition analysis of the bond: (a) OM image, (b) BSD image, (c-d) EDS line scan results.

3.1. IMCs microstructure evolution

Given that the growth of IMCs at room temperature is challenging to observe, high-temperature storage tests were conducted to accelerate their growth. Subsequently, the study delved into the microstructure evolution of IMCs, encompassing phase formation and identification, growth behaviors, and the related growth mechanism.

3.1.1. Phase formation and identification

The bond aged 350 °C for 10 hours was selected to characterize the formation the IMCs and identify the unknown phases since the IMCs were obviously observable with no cracks and voids under the optical microscope, as depicted in Fig. 3(a). Three IMCs layers were distinctly visible with different colors at both the core-shell and bonding interfaces. The light blue layer adjacent to the Al side was designated as IMC 1, the middle grey layer as IMC 2, and the yellow layer near the Cu side as IMC 3. The BSD image of the bond was illustrated in Fig. 3(b), where regions marked in blue and red corresponded to the core-shell and bonding interfaces, respectively. EDS line scan results (Fig. 3c-d) revealed that Cu/Al atoms were distributed in three-step platforms at the interfacial transitional area, aligning well with the positions of the IMC layers. A slight oxygen concentration around the contact area suggested minimal interference with the Cu/Al mutual diffusion process.

To further identify the atomic composition of the IMCs layer, EDS point scanning was performed. The results in Table 1 inferred that IMC 1, IMC 2, and IMC 3 correspond to CuAl_2 , CuAl , and Cu_9Al_4 , respectively.

Considering the limitations of EDS, the TEM analysis was considered as a more accurate verification method for microstructures. Two grains from each IMC layer of the core-shell interface were selected to obtain the SAED patterns. By calibrating the diffraction pattern shown in Fig. 4 (c-h), IMC 1, 2, and 3 were determined to be CuAl_2 (Tetragonal), CuAl (Monoclinic), and Cu_9Al_4 (Cubic), respectively. Fig. 4 presented the lattice information of each IMC with the high-resolution TEM (HRTEM) and Fourier transformation (FFT) images, which was consistent with (110) CuAl_2 , (001) CuAl , and (100) Cu_9Al_4 . Fig. 5

3.1.2. The characterizations of the IMCs growth behaviors

In an attempt to investigate the IMCs growth behaviors and the related mechanisms, the morphologies of the IMCs of the bond aged at 350 °C with various annealing times were also recorded in Fig. 6. It was apparent that the growth of IMCs was non-uniform, and the copper-rich phase Cu_9Al_4 exhibited a more irregular scallop shape near the copper side in comparison with the remaining two phases. As the aging time increased, the thickness of all the diffusion layers grew. Among the IMC phases, Cu_9Al_4 presented the greatest layer thickness, while CuAl possessed the least layer thickness. These observations were attributed to the varying growth characteristics associated with the physical properties of different IMC phases, such as grain size and phase stability.

In addition, the comparison for the bonds aged for 100 hours at different temperatures was also conducted to study the impact of the temperature on IMCs growth, and the characterizations were presented in Fig. 7(a-f). Considering the non-uniform growth of IMC thickness, five measurements were taken for each layer based on SEM images to calculate the average thickness of each Cu/Al IMC. It showed that the thickness of all the diffusion layers became thicker when the aging

Table 1

EDS Point Results of the IMCs at the Core-Shell Interface and Bonding Interface.

Point	A	A'	B	B'	C	C'
Cu (at%)	32.67	32.59	48.80	48.99	62.54	60.76
Al (at%)	65.41	65.41	49.19	49.07	35.65	37.22
O (at%)	1.92	1.99	2.00	1.93	1.81	2.01
Predicted Phase	CuAl_2	CuAl_2	CuAl	CuAl	Cu_9Al_4	Cu_9Al_4

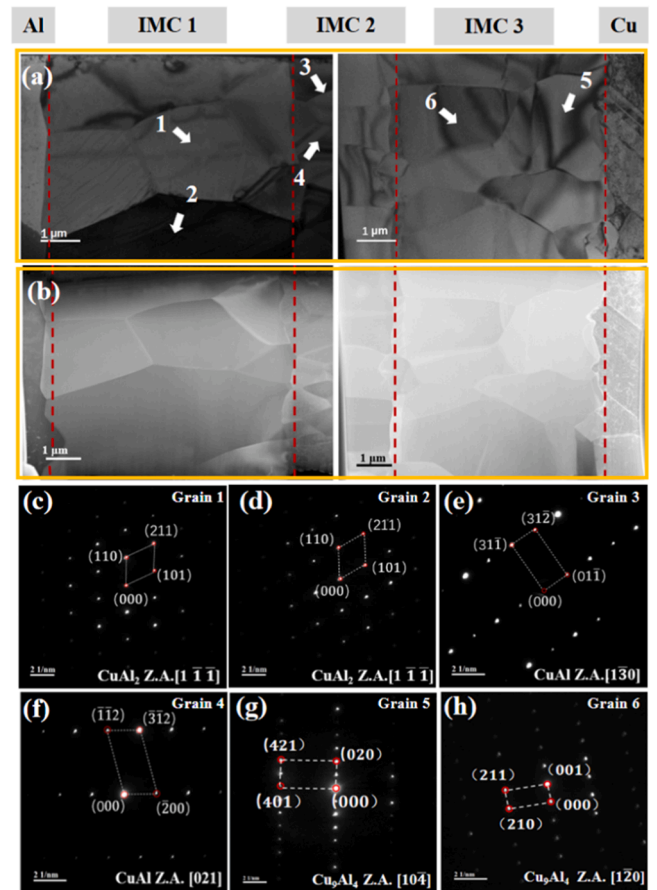


Fig. 4. The TEM analysis of the IMCs at the core-shell interface: (a) TEM images, (b) STEM images, (c-h) SAED patterns and calibrating results of each IMC phase.

temperature increased from 250 °C to the 350 °C. The thickness of CuAl_2 changed from 3.44 μm to the 16.70 μm with the percentage increase of 385 %, while the thickness of Cu_9Al_4 manifested the largest increasing rate of 1402 %, indicating that Cu_9Al_4 is the most temperature-sensitive of all IMCs (Fig. 7g).

3.1.3. The occurring sequence and growth mechanism of IMCs

To date, numerous numerical models and theories have been introduced and developed to decipher the intricate initial phase and formation sequence of IMCs. Among these, the Effective Heat of Formation (EHF) Rule, presented by Pretorius et al. [32], has demonstrated efficacy in predicting the initial phase within the X-Al binary system, as corroborated by several researchers [37–41]. The effective heat formation is mathematically articulated as Eq. (1).

$$\Delta H' = \Delta H^\circ \frac{C_e}{C} \quad (1)$$

where the $\Delta H'$ represents the effective heat of formation of the compound, ΔH° denotes the standard formation heat of the compound, C_e signifies the effective concentration of the limiting element, and C represents the nominal concentration of the limiting element in the compound. Guo et al. [33] applied this model to the Cu/Al binary system, calculating the EHF value for each IMC phase, as detailed in Table 2.

The results indicate that the CuAl_2 phase exhibits the maximum negative EHF, followed by the CuAl phase, while the Cu_9Al_4 phase has the minimum negative EHF. This suggests that CuAl_2 is anticipated to be the initial phase to appear at the interface from a thermodynamic perspective.

In the solid-solid state diffusion system, the thickness of IMCs follows

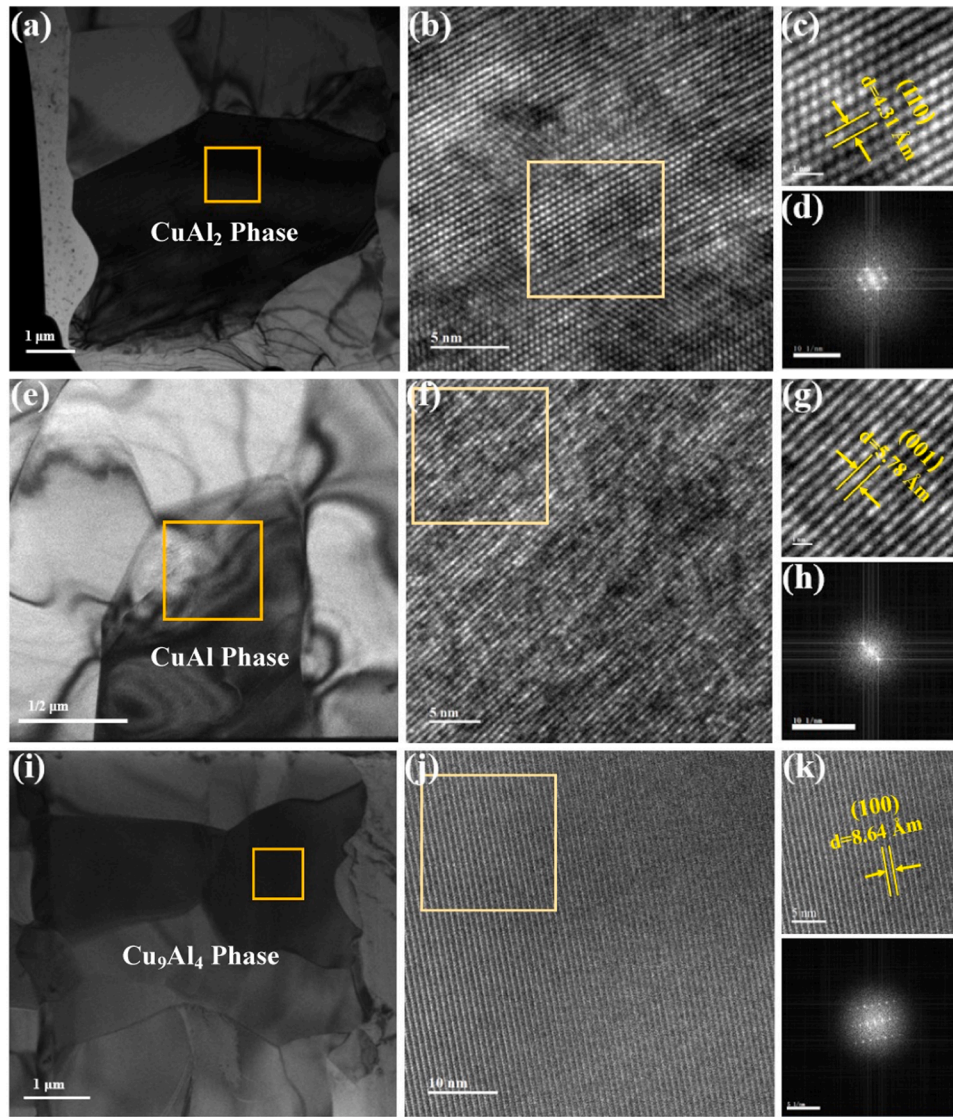


Fig. 5. Morphology and lattice information of IMCs: (a, e, i) TEM images, (b, f, j) HRTEM images, (c, g, k) magnified HRTEM images patterns, (d, h, l) corresponding FFT patterns.

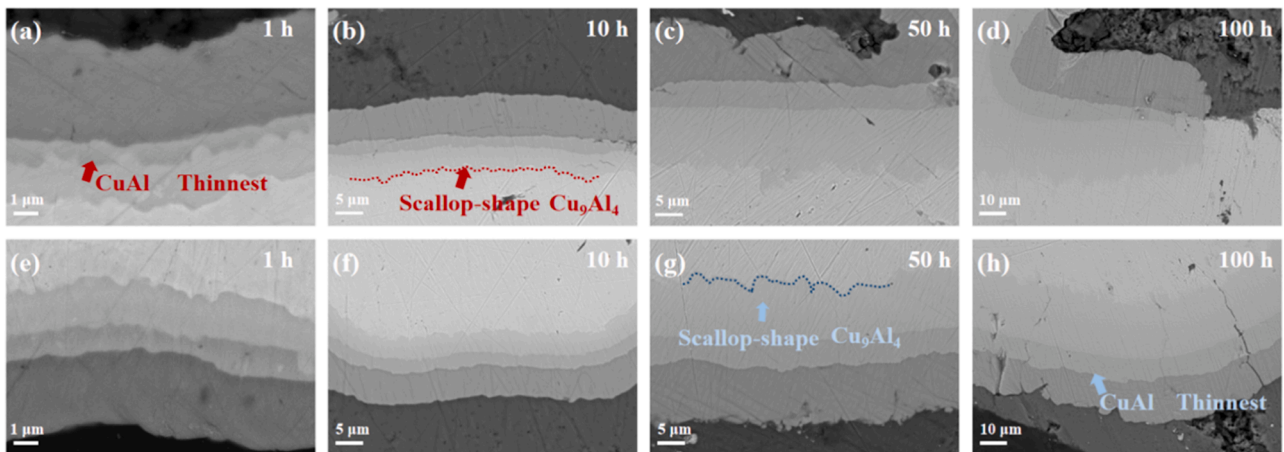


Fig. 6. The evolution of IMCs of the bond aged at 350 °C (a-d) at the bonding interface, (e-h) at the core-shell interface.

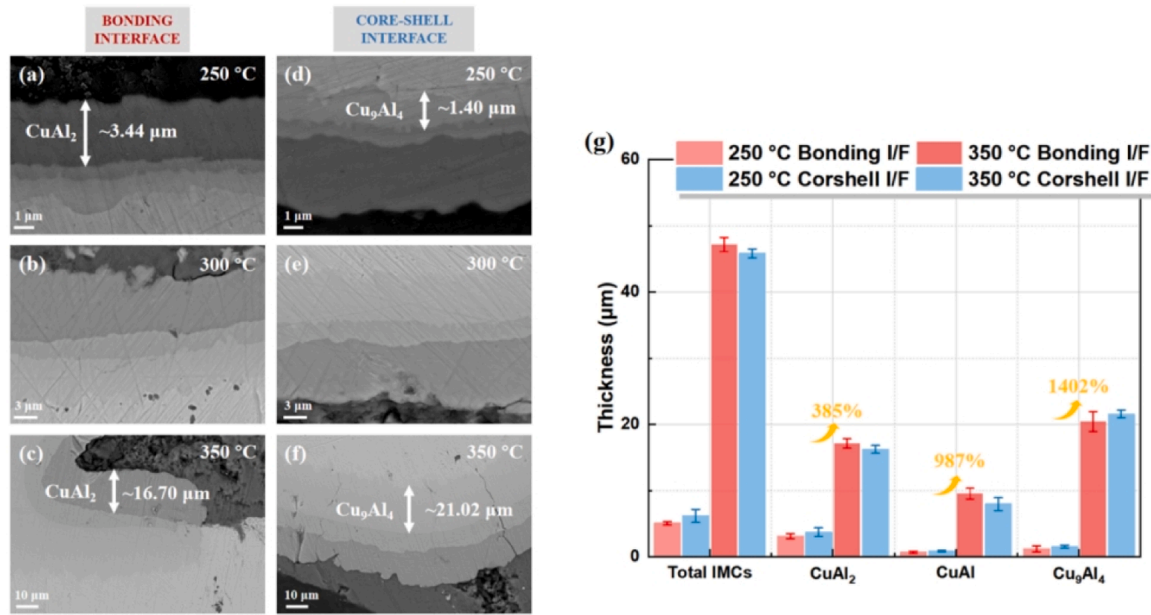


Fig. 7. (a-f) the morphological characterization of the IMCs with various temperatures, (g) the comparison of the IMCs thickness under different temperatures.

Table 2

The effective heat of formation of each IMC phase [33].

IMC Phase	ΔH^f (kJ/mol)	ΔH^i (kJ/mol)
CuAl ₂	-13.05	-6.76
CuAl	-19.92	-6.68
Cu ₉ Al ₄	-21.69	-5.61

the empirical formula listed as Eq. (2):

$$X = (Dt)^{\frac{1}{n}} \quad (2)$$

where X represents the growth thickness of IMCs (m), D is the growth rate of IMCs (m²/s), t is the growth time (s), and n is the time index. When diffusion is controlled by the interfacial reaction, n is expected to be 1. Likewise, when volume diffusion, or lattice diffusion, is the primary mechanism governing IMCs' formation and evolution, n is expected to be 2. As the value of n increases, the growth principle of IMCs becomes more intricate. In this scenario, atoms also diffuse through the grain boundary. The grain boundary gradually fills with diffused atoms over time, resulting in a decrease in the boundary's number and an increase in the n value.

In this experimental investigation, a correlation was observed wherein the thickness of IMCs presented a proportional relationship with the square root of aging time, implying that the n value equals 2. As illustrated in Fig. 8, a parabolic growth pattern revealed that volume diffusion was the predominant mechanism governing the formation and growth of IMCs during the Cu/Al mutual diffusion process.

Moreover, the growth rates of IMC phases under varying temperature conditions were further quantified in Table 3. Notably, under lower-temperature conditions, the growth rate of CuAl₂ surpassed the other phases, aligning coherently with the hypothesis that CuAl₂ was the initial phase. As temperatures escalated, all IMCs shown augmented growth rates, with Cu₉Al₄ emerging as the fastest-growing phase at 350 °C. CuAl consistently manifested a minimal growth rate throughout the temperature spectrum, markedly lower than other phases, resulting in the thinnest CuAl layer.

According to the diffusion theory, the diffusion behavior is further presented by the Arrhenius equation as follows:

$$D = D_0 \exp\left(-\frac{Q}{RT}\right) \quad (3)$$

Where D_0 is the pre-factor, Q is the activation energy, R is the mole gas constant, and T is the aging temperature. The relationship between the growth rate ($\ln(D)$) of the IMC phases and the temperature ($1/T$) was shown in Fig. 9(a). Moreover, the activation energy of IMCs was determined from the slope of the images, as presented in Fig. 9(b). The result for the bonding interface was slightly higher than the value for the core-shell interface, suggesting that IMCs at the latter interface might appear earlier than those at the former interface. Notably, the aluminum-rich phase CuAl₂ owned the lowest activation energy, aligning with its preference as the initial phase, consistent with the EHF rule. Meanwhile, it was observed that the activation energy of the wedge bonds in thick wires in this study (111 kJ/mol for the bonding interface and 106 kJ/mol for the core-shell interface) is evidently higher than the documented results for ball bonds in thin wires (20–70 kJ/mol) [21]. This disparity can be attributed to the substantial increase in the contact area at the interface, requiring more energy for the IMCs to overcome the contact crystal lattice and facilitate their formation and growth.

According to the analysis discussed above, the general total IMCs growth rules were expressed as Eq. (4) and Eq. (5) for the core-shell interface and the bonding interface, respectively. The modulation of the IMCs thickness was achieved which helped the engineers fabricate the wire bond with better performance.

$$X^2 = t3.4 \times 10^{-6} \exp\left(-\frac{12751.9846}{T}\right) \quad (4)$$

$$X^2 = t1.1 \times 10^{-5} \exp\left(-\frac{13401.4915}{T}\right) \quad (5)$$

In accordance with Eqs. (4) and (5), the diffusion coefficient at the core-shell interface was smaller than that at the bonding interface. However, the activation energy at the core-shell interface was lower, facilitating the formation of IMCs. Consequently, the final IMCs thickness at the two interfaces exhibited minor differences.

In the investigation of microstructure evolution of the IMCs, CuAl₂, CuAl, Cu₉Al₄ were identified to be the appeared phases. Among them, the scallop-shape phase Cu₉Al₄ was most sensitive to the temperature variations. The parabolic relationship between the IMCs thickness and

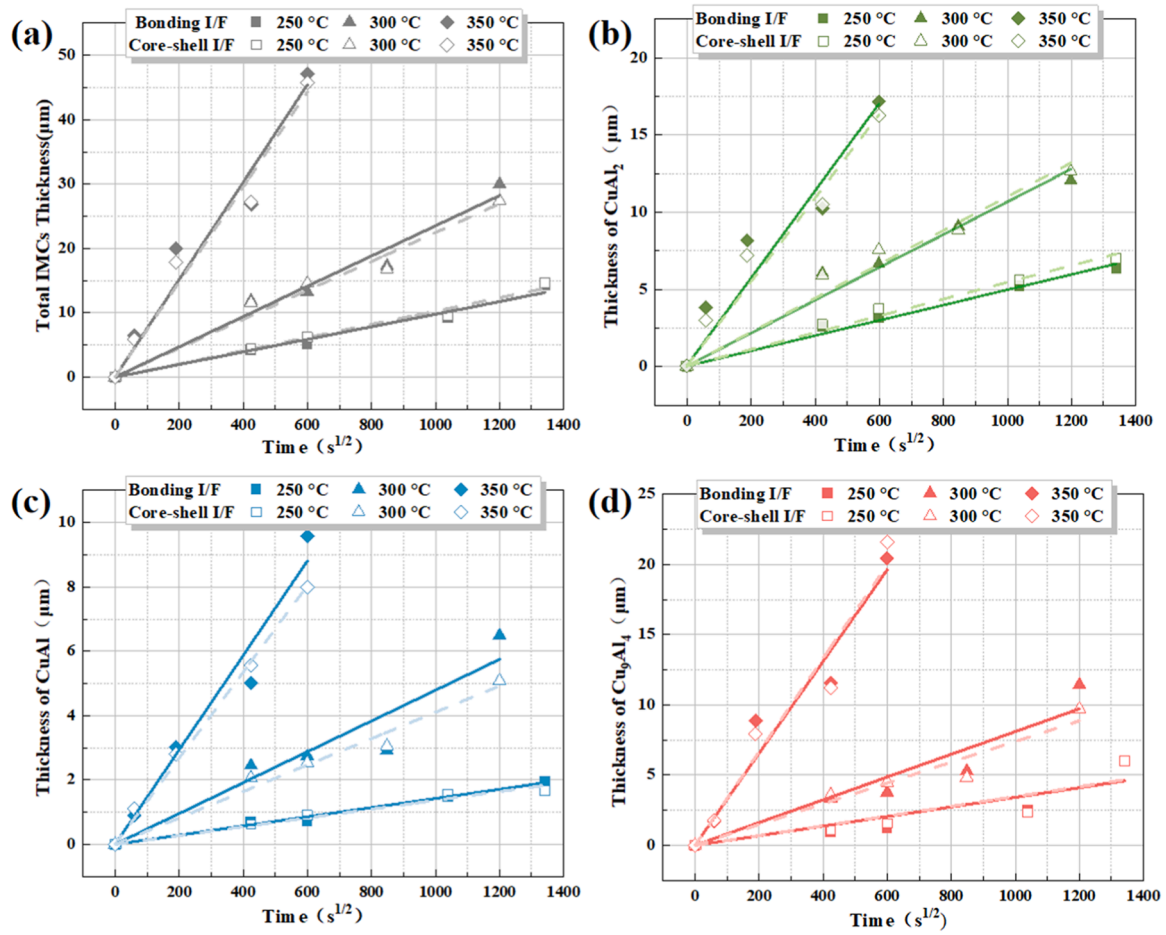


Fig. 8. Relationship between IMCs thickness and the square root of aging time.

Table 3

Growth rates of IMCs at the core-shell interface and the bonding interface.

Growth Rate ($10^{-16} \text{ m}^2/\text{s}$)	Total IMCs		CuAl_2		CuAl		Cu_9Al_4	
	Corshell	Bonding	Corshell	Bonding	Corshell	Bonding	Corshell	Bonding
250 °C	0.96	1.05	0.24	0.29	0.02	0.02	0.12	0.12
300 °C	5.53	5.04	1.13	1.20	0.23	0.17	0.66	0.55
350 °C	60.17	54.52	8.00	7.36	2.16	1.79	10.71	11.11

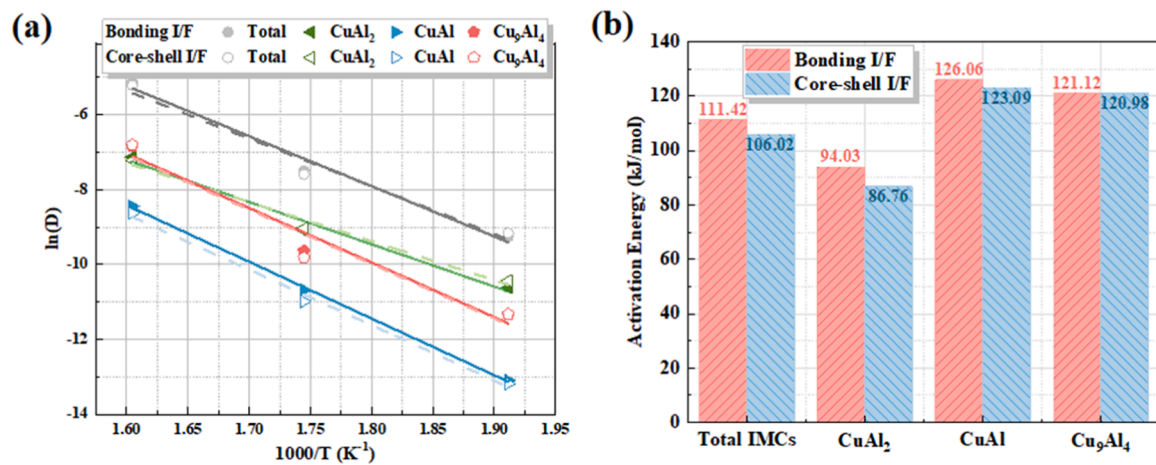


Fig. 9. (a) Relationship between the growth rate and the aging time, (b) the calculated activation energies of IMCs.

aging time revealing that the volume diffusion controlled the growth of the IMCs. The bonding interface showed a slightly higher activation energy compared to the core-shell interface, implying that IMCs formation is relatively more challenging at the bonding interface.

3.2. The relationship between the mechanical properties of the bonds and the IMCs

The thickness of IMCs significantly impacts the bondability of wire bonds due to intrinsic physical properties such as hardness, thermal conductivity, and coefficient of thermal expansion (CTE). An optimal thickness range is believed to enhance the mechanical strength of the bond, given that IMCs generally exhibit higher hardness than base materials. However, excessive growth results in a substantial decrease in mechanical reliability due to increased ductility. Therefore, mechanical

tests, including shear and pull tests, were conducted to assess the changes in bond reliability under various high-temperature aging conditions.

Fig. 10 (a-c) presented that the results obtained across varied temperature conditions exhibited consistent tendencies, which were categorized into three successive stages. In the initial stage, occurring in an oxygen-rich high-temperature setting, a copper oxide layer of specific thickness developed on the surface. This layer served as a barrier, impeding the mutual diffusion of copper and aluminum atoms. Additionally, the significant difference in CTE between copper oxides and the copper substrate resulted in an overall reduction in the shear and tensile strength of the bonds. Advancing to the second stage, the diffusion of copper and aluminum atoms intensified, leading to the formation and growth of Cu/Al IMCs. The physical properties of IMCs progressively enhance the mechanical strength of the contact interface. As the aging

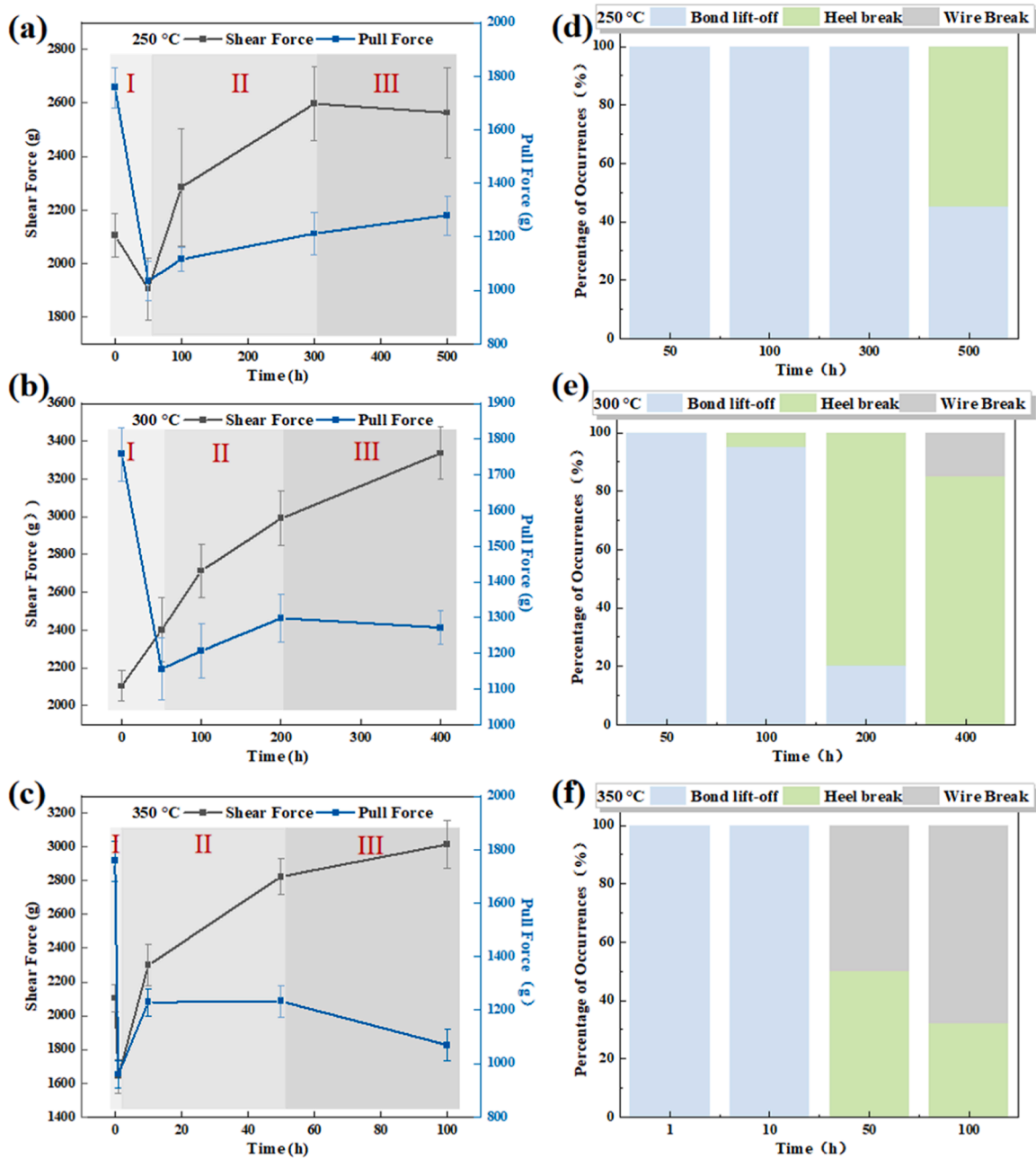


Fig. 10. (a-c) Results of shear and pull tests for wire bonds aged under different temperatures with varying aging times, (d-f) Results of the failure mode of the bonds during the pull test.

time progresses into the final stage, the thickness of IMCs kept increasing, and cracks and voids may emerge at the interface due to the mismatch between the CTE of IMCs and copper, as well as the different diffusion rates of copper and aluminum atoms (Kirkendall Effect). This occurrence diminishes the anti-shear and anti-pull capabilities and further deteriorates the overall performance of the bonds.

Furthermore, the failure mode of bond wire in each temperature group was documented in Fig. 10 (d-f). Across the duration of the experiment, three distinct failure modes were identified: bond lift-off, indicating complete detachment of the bond from the substrate surface; heel break, where the fracture occurs in the neck region with significant deformation due to the shape of the wedge bonder, and the bond point remains still affixed to the substrate; and wire break, indicating that the fracture occurs in or near the middle of the wire. Observations presented a shift in the failure mode of the bonds with an increase in aging temperature and time. The transition progressed from bond lift-off to heel break and ultimately to wire break mode. This evolution aligns with the gradual formation and growth of IMCs during the aging process, underscoring the notable impact of IMCs growth on the reliability of wire bonds.

In the investigation of the relationship between the mechanical properties of the bonds and the IMCs, a discernible trend was observed. Initially, there was a decrease in the mechanical properties of bonding points, succeeded by an increase, and subsequently followed by another decrease with the extension of the IMCs thickness. The tensile failure mode gradually transitioned towards wire break as the IMCs overgrew, impacting the mechanical reliability of the bonds.

3.3. The molecular dynamics simulation of interdiffusion

In this work, models with varying material characteristics were established to investigate the effects of the crystalline state of Cu/Al materials on interdiffusion at the atomic scale, subsequently revealing and verifying the diffusion mechanisms in bi-polycrystalline materials from a simulation perspective.

3.3.1. The investigation of influence materials type on the diffusion process

As documented, atomic diffusion across interfaces typically occurs at sufficiently high temperatures, commonly ranging from 0.6 to 0.8 times the material's melting point [25,27]. Given that the melting point of copper is 1356 K and aluminum is 933 K, the simulations were conducted at 750 K for 400 ps to ensure adequate diffusion of Cu and Al atoms into each other.

Fig. 11 illustrated the diffusion process of models with various crystalline states of materials (Model A was the bi-monocrystalline model, Models B and C were hybrid models, and Model D was the bi-polycrystalline model). To reflect the interior diffusion process of the materials body instead of focusing on the outer surfaces of the models, the Selected Atoms Module in OVITO was utilized to ensure that each slab contained only one type of element, and then the polycrystalline models were rendered by 'grain ID' in Color Coding Module (as depicted on right of sub-figure). These slabs have been shifted to enhance the visibility of the interior interdiffusion process. It demonstrated that the crystalline state of copper material significantly influenced the mutual diffusion process. Specifically, the diffusion level was more intense in the polycrystalline copper model compared to the monocrystalline models, whereas there was only a slight difference between the results of the polycrystalline aluminum and monocrystalline aluminum models. Additionally, the copper atoms dominated the interdiffusion process regardless of the material nature, while aluminum atoms tended to remain unchanged at the initial surface. This observed variation can be attributed to several factors. Firstly, the lower melting point of aluminum facilitates the breaking of Al-Al bonds and the creation of vacancies, providing favorable conditions for copper atom diffusion. Secondly, the smaller atomic radius of copper (1.28 Å) compared to aluminum (1.43 Å) allows for easier diffusion into the aluminum matrix. Lastly, in polycrystalline materials, atoms at grain boundaries are more likely to participate in diffusion movements due to its high energy state, accelerating the diffusion process.

3.3.2. Calculation of mean square displacement (MSD) and diffusion coefficient of Cu/Al atoms

To further investigate the detailed the diffusion behaviors and

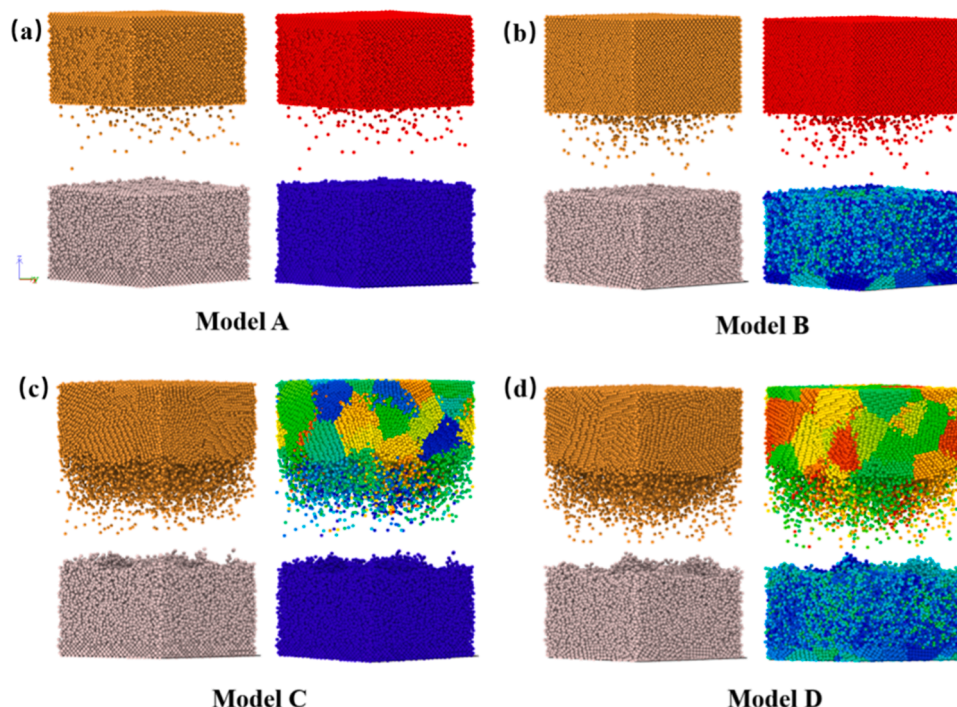


Fig. 11. The snapshots of Cu/Al mutual diffusion with various material natures at 750 K after simulation for 400 ps.

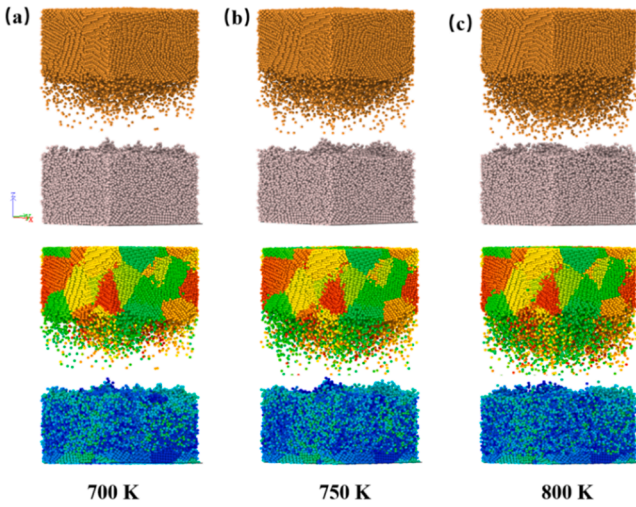


Fig. 12. The Snapshots of Cu/Al mutual diffusion obtained at different temperatures after simulation for 400 ps.

mechanism between the Cu and Al atoms, the bi-polycrystalline model was selected for the following research, as it better reflected real-life applications. The simulations were conducted at the 700 K, 750 K, and 800 K, respectively for a duration of 400 ps and the results were visualized in Fig. 12.

As the temperature increased, the disorder of copper and aluminum atoms intensified, and the diffusion phenomenon became more pronounced. Then, the diffusion characteristics of the Cu and Al atoms were further quantified by the calculation of the mean square displacement of copper and aluminum atoms was calculated by applying Eq. (6) and the relationship between *MSD* and time was depicted in Fig. 13 to analyze the movement of atoms at the interface.

$$MSD = \langle r^2(t) \rangle = \frac{1}{N} \sum_{i=1}^N (|r_{z_i}(t) - r_{z_i}(0)|^2) \quad (6)$$

Where $\langle \rangle$ means to average the physical quantity in brackets at time t , r is the atomic position vector, and N is the total number of atoms in the simulation system.

The mean square displacement of aluminum atoms was significantly larger than that of copper atoms at the same temperature, suggesting more intense movement of aluminum atoms. The maximum mean square displacement for both copper and aluminum atoms increased

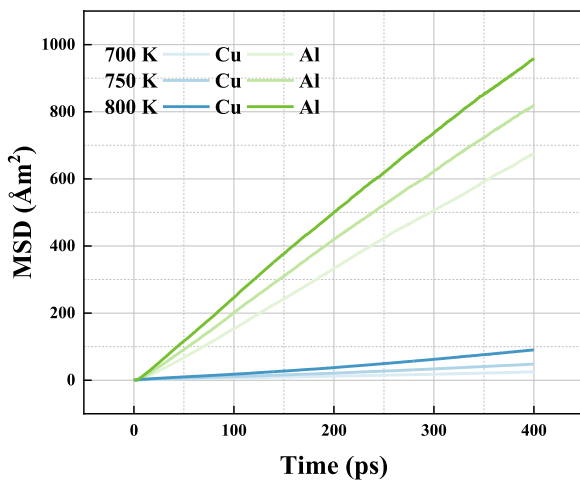


Fig. 13. Relationship between the *MSD* of Cu (Al) atoms and the simulation time.

with rising temperature, indicating that more atoms acquire sufficient energy to overcome the energy barrier. In essence, the hopping frequency of atoms rose with increasing temperature, rendering the diffusion phenomenon more prominent.

In accordance with the Einstein diffusion law, the diffusion coefficient, representing the speed of atom diffusion, is expressed as follow:

$$D = \lim_{t \rightarrow \infty} \frac{1}{2\tilde{N}t} \langle |r_{z_i}(t) - r_{z_i}(0)|^2 \rangle \quad (7)$$

where \tilde{N} is the dimensionality of the system, and r is the atomic position vector. As the diffusion in the simulation model occurred only in one dimension (z -direction), the diffusion coefficient was effectively half of the slopes of the *MSD*- t plots. The obtained results at the specified temperatures were presented in Table 4. In all simulations, the diffusion rate of aluminum atoms was greater than that of copper atoms. However, the diffusion rate of the copper atoms increased more rapidly as the temperature rose since copper was the predominant diffusing element.

In summary, it can be concluded that the application of polycrystalline copper significantly enhances interdiffusion at the Cu/Al interface. During the diffusion process, Cu atoms exhibited a tendency to diffuse into the interior of the Al layer, albeit at a slower rate, while most Al atoms encountered difficulties penetrating the Cu layer, despite their higher diffusion rate.

3.3.3. Simulation verification of atomic diffusion mechanism

The diffusion layer, also referred to as the intermetallic compounds formed at the interface, usually displays the different characteristics of the base materials. However, there is limited research on the formation and growth of IMCs at the interface at the atomic level based on the molecular dynamics. In this study, the parabolic relationship between the diffusion layer thickness and aging time was revealed and validated the growth empirical rule we discussed in experiments.

The thickness of the interfacial region is determined from the concentration profile, where concentrations exceeding 5 % is defined as the interfacial region [25,28]. Fig. 14 presented the concentration profiles of copper and aluminum atoms along the vertical axis under various simulated annealing temperatures, with the diffusion layer boundaries demarcated by grey dotted lines. It shows that the thickness of the diffusion layer increased from 33.41 Åm at 700 K to 40.74 Åm at 800 K. Notably, as the annealing temperature increased, the left boundary of the diffusion region shifted towards the aluminum side, contracting from 44.61 Åm to 31.95 Åm, while the right boundary expanded towards the copper side, increasing from 78.02 Åm to 84.55 Åm. These observations demonstrated that copper was the dominant diffusing element, with the predominant diffusion direction being from the copper side towards the aluminum side. Moreover, the boundary shifted were more pronounced between 750 K and 800 K compared to 700 K to 750 K, indicating a significant intensification of the diffusion process at higher temperatures. This suggested that the optimal temperature range for efficient Cu/Al mutual diffusion occurred at temperatures above 750 K.

To quantitatively illustrate the mutual diffusion process, concentration profiles under various annealing temperatures were input into MATLAB (2023a) to calculate the interdiffusion coefficients of each Cu/Al intermetallic compound (IMC) phase using the Matano method as follows[34]:

Table 4

The diffusion coefficient of Cu and Al atoms under different simulated temperatures.

Temperature (K)	D_{Cu} (m^2/s)	D_{Al} (m^2/s)
700	2.86×10^{-10}	8.70×10^{-9}
750	5.78×10^{-10}	1.04×10^{-8}
800	1.11×10^{-9}	1.22×10^{-8}

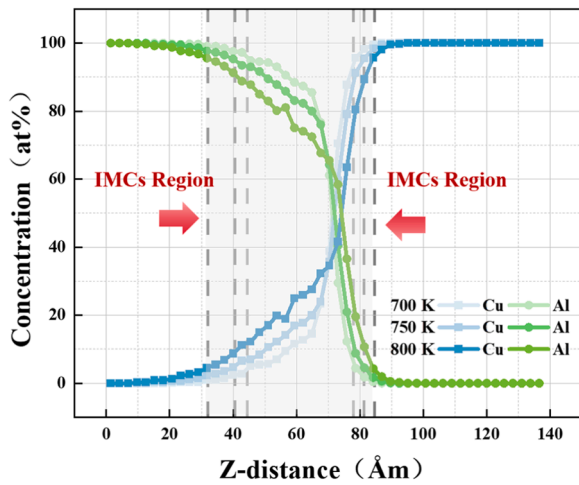


Fig. 14. The concentration distribution of copper and aluminum atoms along the z-direction after simulation for 400 ps.

$$\tilde{D}(c) = -\frac{1}{2t} \frac{dx}{dc} \int_0^c xdc \quad (8)$$

With $\int_0^c xdc = 0$ and where $\tilde{D}(c)$ is the interdiffusion coefficient of the IMC phase of concentration c , x is the distance from the initial interface and t is the diffusion time. By determining the Matano plane, the interdiffusion coefficients for each IMC phase were derived from Eq. (8), with the results listed in Table 5. It was observed that the interdiffusion coefficients of each IMC increased as the temperature rose from 700 K to 800 K, leading to an expansion of the diffusion region thickness. Among the results, CuAl_2 , as the initial phase, exhibited the highest interdiffusion rate, indicating its dominant role in the diffusion process. In contrast, the CuAl and Cu_9Al_4 phases displayed similar interdiffusion rates. This finding aligned well with the activation energy discussion presented in Fig. 9(b).

As illustrated in Fig. 15, the square of the diffusion layer thickness exhibited a well-defined linear function relationship with simulation time, which aligned closely with the conclusions drawn from the experiments discussed in the previous section, validating that the diffusion process at the interface between Cu and Al is controlled by volume diffusion, that is, vacancy diffusion.

The calculated growth rates from simulations were further compared with the experimental results in Table 6. The simulation results were significantly higher than the actual experimental values. This disparity can be attributed to several factors. Firstly, the simulated interfacial diffusion in this study assumed pure metals without defects, and the contact plane was ideal with no roughness or oxidation, whereas these real complexities were not considered in the simulation. Secondly, the atomic density gradient from the surface to the interior crystal body, present in actual scenarios, was not accounted for in our simulation, potentially contributing to the accelerated diffusion process. The final simulated activation energy was determined to be 41 kJ/mol.

To further investigate the Cu/Al mutual diffusion, Fig. 16 summarized the activation energies derived from both experimental and simulated data in this study, alongside comparisons with values reported in previous research [21,33,35–41]. The results indicated notable variations in activation energy across different studies, which could be

Table 5
The simulated interdiffusion coefficients of Cu/Al IMCs.

Temperature (K)	$\tilde{D}_{\text{CuAl}_2}(\text{m}^2/\text{s})$	$\tilde{D}_{\text{CuAl}}(\text{m}^2/\text{s})$	$\tilde{D}_{\text{Cu}_9\text{Al}_4}(\text{m}^2/\text{s})$
700	4.7×10^{-10}	2.60×10^{-10}	2.29×10^{-10}
750	7.9×10^{-10}	4.86×10^{-10}	4.60×10^{-10}
800	1.09×10^{-8}	7.83×10^{-10}	6.84×10^{-10}

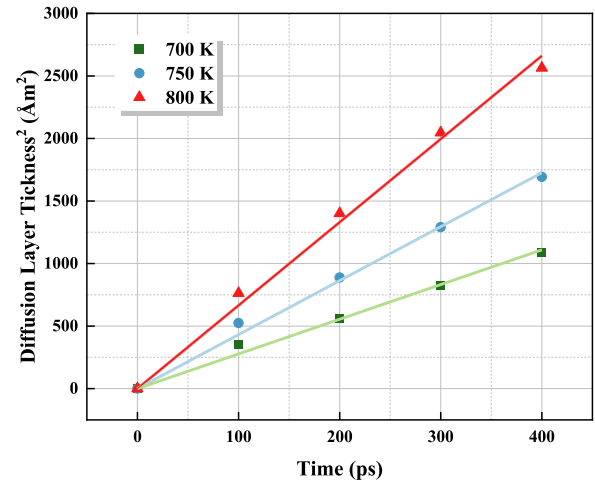


Fig. 15. Relationship between the square of IMCs thickness and the simulation time.

Table 6
Comparison of the growth rate between experimental and simulated results.

Temperature (K)	$D_{\text{simulation}} (\text{m}^2/\text{s})$	$D_{\text{actual-prediction}} (\text{m}^2/\text{s})$	
		Corshell	Bonding
700	2.7×10^{-8}	1.4×10^{-13}	1.9×10^{-13}
750	4.3×10^{-8}	4.6×10^{-13}	5.7×10^{-13}
800	6.6×10^{-8}	10.3×10^{-13}	15.4×10^{-13}

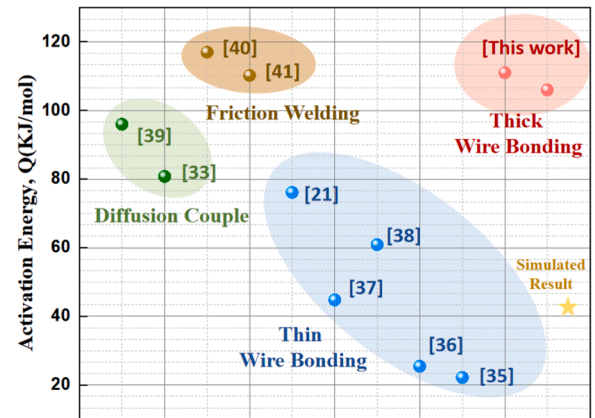


Fig. 16. Comparison of activation energies of Cu/Al IMCs reported in the literature.

attributed to variations in fabrication techniques, matrix materials, annealing conditions, and analytical methodologies. In wire bonding technology, compared to ball bonds made with thin wires, the activation energy of wedge bonds made with thick wires in this work exhibited higher values, likely due to the increased contact area at the interface, which requires more energy for atoms to overcome the more intact crystal lattice. While the simulated activation energy was notably lower, as previously discussed, this discrepancy may arise from the idealized conditions assumed in molecular dynamics simulations, which often do not account for the complexities present in experimental setups, such as defects and impurities in polycrystalline materials.

In the investigation of molecular dynamics simulation of Cu/Al mutual diffusion, the polycrystalline models presented the intensive diffusion phenomenon than the monocrystalline ones and copper emerged as the predominant diffusion element. The simulation results based on the quadratic relationship between IMCs thickness and

simulation time further corroborated the volume diffusion mechanism governing the growth of Cu/Al IMCs.

4. Conclusions

The growth of intermetallic compounds at the Cu/Al interface significantly influences the reliability of bonds, necessitating an in-depth study of IMC formation, evolution, and growth mechanisms. This study focused on ultrasonic wedge bonds involving thick wires, which significantly differ in wire diameters and bond deformation degree from ball bonds. In this investigation, precise regulation of IMCs thickness was achieved through SEM-EDS, TEM, and SAED analysis, while comprehensive mechanical properties characterization was conducted to evaluate bonding interface strength. Additionally, dynamic observation of atomic diffusion through molecular dynamic simulations explored the micro-diffusion behaviors at the Cu/Al interface. The conclusions drawn from this study are as follows.

(1) IMCs Morphology and Growth Mechanism: IMCs layer thickness increased with time, as observed through OM and SEM images. CuAl_2 , CuAl , and Cu_9Al_4 were identified as the appearing phases by further analysis. CuAl_2 grew fastest in the low-temperature group, and Cu_9Al_4 exhibited a faster growth trend in the high-temperature group, while CuAl remained the slowest growth rate during all of the annealing experiments. The overall IMC growth rate at the core-shell interface was slightly faster than at the bonding interface. According to the SEM images, it was revealed that there was a linear relationship between IMCs thickness and the half power of time, presenting that the growth of Cu/Al IMCs was governed by the volume diffusion mechanism.

(2) Mechanical Properties: Mechanical tests indicated three stages in the changing trend of shear and tensile strength, dominated by the generation of copper oxides, IMCs, and cracks and voids in respective stages. The failure mode in the tensile tests shifted from bond detachment to neck fracture and then to wire break with aging time extension.

(3) Atomic Diffusion Simulation: The substantial impact of material characteristics on the mutual diffusion between Cu and Al atoms was highlighted through the molecular dynamics simulations. Specifically, the bi-polycrystalline model showed the most pronounced diffusion results. Despite its comparatively lower diffusion coefficients, copper atoms emerged as the predominant element during the diffusion process. The simulations also validated the parabolic relationship between IMCs thickness and time, suggesting that the volume diffusion was the main mechanism in the Cu/Al interdiffusion.

In summary, this study integrates macro-experimentation and micro-simulation to discuss the comprehensive IMCs growth mechanism and formulate detailed relationships. The revealed correlation between IMCs thickness and mechanical performance provides insights for fabricating wire bonds with enhanced reliability, fostering the application of novel composite materials in high-temperature packaging.

Funding

This study was supported by the National Natural Science Foundation of China under Grant 62304051, the Research Institute of Fudan University in Ningbo (Ningbo Science & Technology Innovation 2025 Major Project 2022Z089), Shanghai SiC Power Devices Engineering & Technology Research Center (19DZ2253400) and Heraeus Materials Technology Shanghai Ltd.

CRedit authorship contribution statement

Wenting Liu: Writing – original draft, Methodology, Formal analysis. **Xinyue Wang:** Methodology, Investigation, Data curation. **Jing Zhang:** Writing – review & editing, Supervision, Resources. **Guoqi Zhang:** Supervision. **Pan Liu:** Writing – review & editing, Supervision, Project administration, Funding acquisition, Conceptualization.

Declaration of Competing Interest

The authors declare that they have no known competing financial interests or personal relationships that could have appeared to influence the work reported in this paper.

Acknowledgements

In this work, the authors would like to thank the National Natural Science Foundation of China under Grant 62304051, the Research Institute of Fudan University in Ningbo (Ningbo Science & Technology Innovation 2025 Major Project 2022Z089), and Shanghai SiC Power Devices Engineering & Technology Research Center (19DZ2253400) for funding this research on providing simulation support and laboratory accesses. Many thanks to Heraeus Materials Technology Shanghai Ltd. for prototype validation and characterization support, and the Chat Generative Pre-trained Transformer (ChatGPT, OpanAI) for language help.

Data availability

Data will be made available on request.

References

- [1] K. Ravinchandra, et al., Review of wide band-gap technology: power device, gate driver, and converter design, *J. Power Electron.* 22 (2022) 1398–1413, <https://doi.org/10.1007/s43236-022-00470-6>.
- [2] S. Singh, T. Chaudhary, G. Khanna, Recent advancements in wide band semiconductors (SiC and GaN) technology for future devices, *Silicon* 14 (2022) 5793–5800, <https://doi.org/10.1007/s12633-021-01362-3>.
- [3] F. Roccaforte, et al., Emerging trends in wide band gap semiconductors (SiC and GaN) technology for power devices, *Microelectron. Eng.* 187–188 (2018) 66–77, <https://doi.org/10.1016/j.mee.2017.11.021>.
- [4] P.S. Chauhan, A. Choubey, Z. Zhong, M.G. Pecht, *Copper wire bonding (Copper Wire Bonding)*, Springer New York, New York, NY, 2014, pp. 1–9, https://doi.org/10.1007/978-1-4614-5761-9_1.
- [5] N. Ross, et al., Mechanistic study of copper wire-bonding failures on packaging devices in acidic chloride environments, *Microelectron. Reliab.* 113 (2020) 113917, <https://doi.org/10.1016/j.microrel.2020.113917>.
- [6] L.J. Lois et al., Comprehensive study of wire bond reliability impacts from wire, molding compound and bond pad contaminations, 2019 IEEE 21st Electronics Packaging Technology Conference (EPTC), pp. 197–202, <https://doi.org/10.1109/EPTC47984.2019.9026721>.
- [7] H. Yang, Y. Wang, H. Zhang, J. Lu, Y. Lu, Ductile Au_4Al intermetallic compound with crack resistance, *Intermetallics* 112 (2019) 106555, <https://doi.org/10.1016/j.intermet.2019.106555>.
- [8] A. Chen and R. Lo, *Semiconductor Packaging: Materials Interaction and Reliability*, 2016, pp. 1–187, <https://doi.org/10.1201/b11260>.
- [9] L. Li, S. Xu, Y. k Liang, and P. Wei, 10 mils Al wire heavy wedge bond wire deformation thickness study, 2019 20th International Conference on Electronic Packaging Technology (ICEPT), pp. 1–4, <https://doi.org/10.1109/ICEPT47577.2019.9245791>.
- [10] A. Gueydan, B. Domengès, E. Hug, Study of the intermetallic growth in copper-clad aluminum wires after thermal aging, *Intermetallics* 50 (2014) 34–42, <https://doi.org/10.1016/j.intermet.2014.02.007>.
- [11] R. Schmidt, C. König, P. Prenosil, Novel wire bond material for advanced power module packages, *Microelectron. Reliab.* 52 (2012) 2283–2288, <https://doi.org/10.1016/j.microrel.2012.06.139>.
- [12] C. Fang et al., Influence of Al/CuorAl wire bonding on reliability of SiC devices, 2021 IEEE Workshop on Wide Bandgap Power Devices and Applications in Asia (WiPDA Asia), pp. 259–263, <https://doi.org/10.1109/WiPDAAsia51810.2021.9655999>.
- [13] E. Milke, R. Schmidt, and U. Scheuermann, *Al-Clad Cu Wire Bonds Multiply Power Cycling Lifetime of Advanced Power Modules* (PCIM Europe). 2012. [Online]. Available: (<https://www.tib.eu/en/search/id/tema%3ATEMA20130100397>).
- [14] Y. Shajari, et al., Formation of intermetallic compounds in Al–Cu interface via cold roll bonding: review, *Surf. Eng. Appl. Electrochem.* 58 (2022) 41–50, <https://doi.org/10.3103/S1068375522010112>.
- [15] F. Cao, P. Zhang, J. Zou, T. Wang, The formation and growth of intermetallic compounds during interdiffusion of Al/Cu bimetal, *Mater. Res. Express* 9 (2022), <https://doi.org/10.1088/2053-1591/ac69b4>.
- [16] C.L. Cha, H.J. Chong, H.G. Yaw, M.Y. Chong, and C.H. Teo, Cu-Al Intermetallic Growth Behaviour Study Under High Temperature Thermal Aging, 2018 IEEE 38th International Electronics Manufacturing Technology Conference (IEMT), pp. 1–5, <https://doi.org/10.1109/IEMT.2018.8511626>.

- [17] K. Hyoung-Joon, et al., Effects of Cu/Al intermetallic compound (IMC) on copper wire and aluminum pad bondability, *IEEE Trans. Compon. Packag. Technol.* 26 (2003) 367–374, <https://doi.org/10.1109/TCAPT.2003.815121>.
- [18] M.H.M. Kouters, G.H.M. Gubbels, O. Dos Santos Ferreira, Characterization of intermetallic compounds in Cu–Al ball bonds: mechanical properties, interface delamination and thermal conductivity, *Microelectron. Reliab.* 53 (2013) 1068–1075, <https://doi.org/10.1016/j.microrel.2013.02.020>.
- [19] H. Xu, et al., Behavior of aluminum oxide, intermetallics and voids in Cu–Al wire bonds, *Acta Mater.* 59 (2011) 5661–5673, <https://doi.org/10.1016/j.actamat.2011.05.041>.
- [20] C.J. Hang, C.Q. Wang, M. Mayer, Y.H. Tian, Y. Zhou, H.H. Wang, Growth behavior of Cu/Al intermetallic compounds and cracks in copper ball bonds during isothermal aging, *Microelectron. Reliab.* 48 (2008) 416–424, <https://doi.org/10.1016/j.microrel.2007.06.008>.
- [21] C.-P. Liu, S.-J. Chang, Y.-F. Liu, W.-S. Chen, Cu–Al interfacial formation and kinetic growth behavior during HTS reliability test, *J. Mater. Process. Technol.* 267 (2019) 90–102, <https://doi.org/10.1016/j.jmatprotec.2018.12.012>.
- [22] S. Law Chee and V. Krishna, Wire strength of Cu wire on Al metallization after high temperature reliability, 2008 33rd IEEE/CPMT International Electronics Manufacturing Technology Conference (IEMT), pp. 1–5, <https://doi.org/10.1109/IEMT.2008.5507847>.
- [23] S. Xie, P. Lin, and Q. Yao, Overview of Au–Al Bond Interface, 2021 International Conference on Electronics, Circuits and Information Engineering (ECIE), pp. 250–253, <https://doi.org/10.1109/ECIE52353.2021.00060>.
- [24] M. Schneider-Ramelow, S. Schmitz, B. Schuch, and W. Grubl, Kirkendall voiding in Au ball bond interconnects on Al chip metallization in the temperature range from 100 – 200° C after optimized intermetallic coverage, 2009 European Microelectronics and Packaging Conference, pp. 1–6. [Online]. Available: (<https://api.semanticscholar.org/CorpusID:5708763>).
- [25] S. Chen, F. Ke, M. Zhou, Y. Bai, Atomistic investigation of the effects of temperature and surface roughness on diffusion bonding between Cu and Al, *Acta Mater.* 55 (2007) 3169–3175, <https://doi.org/10.1016/j.actamat.2006.12.040>.
- [26] J. Yang, J. Zhang, J. Qiao, Molecular dynamics simulations of atomic diffusion during the Al–Cu ultrasonic welding process, *Materials* 12 (2019) 2306. (<https://www.mdpi.com/1996-1944/12/14/2306>) [Online]. Available).
- [27] M. Zaenudin, A.H.A. Gaffar, M.N. Mohammed, M.A.M. Ali, O.I. Al-Sanjary, and S. Al-Zubaidi, Study the Effect of Temperature on the Diffusion Bonding of Cu–Al by Using Molecular Dynamics Simulation, 2019 IEEE International Conference on Automatic Control and Intelligent Systems (I2CACIS), pp. 345–348. <https://doi.org/10.1109/I2CACIS.2019.8825068>.
- [28] C. Li, D. Li, X. Tao, H. Chen, Y. Ouyang, Molecular dynamics simulation of diffusion bonding of Al–Cu interface, *Model. Simul. Mater. Sci. Eng.* 22 (2014) 065013, <https://doi.org/10.1088/0965-0393/22/6/065013>.
- [29] R.W. Hockney, The potential calculation and some applications. [Online]. Available: (<https://api.semanticscholar.org/CorpusID:117901330>).
- [30] D.J. Evans, B.L. Holian, The nose–hoover thermostat, *J. Chem. Phys.* 83 (1985) 4069–4074. (<https://api.semanticscholar.org/CorpusID:94786326>) [Online]. Available).
- [31] J. Cai, Y.Y. Ye, Simple analytical embedded-atom-potential model including a long-range force for fcc metal and their alloys, *Phys. Rev., B Condens* 54 (1996) 8398–8410. (<https://doi.org/10.1103/PhysRevB.54.8398>).
- [32] R. Pretorius, T.K. Marais, C.C. Theron, Thin film compound phase formation sequence: An effective heat of formation model, *Mater. Sci. Rep.* 10 (1993) 1–83, [https://doi.org/10.1016/0920-2307\(93\)90003-W](https://doi.org/10.1016/0920-2307(93)90003-W).
- [33] Y. Guo, G. Liu, H. Jin, Z. Shi, G. Qiao, Intermetallic phase formation in diffusion-bonded Cu/Al laminates, *J. Mater. Sci.* 46 (2011) 2467–2473, <https://doi.org/10.1007/s10853-010-5093-0>.
- [34] Y. Funamizu, K. Watanabe, Interdiffusion in the Al–Cu System, *Mater. Trans.* 12 (1971) 147–152, <https://doi.org/10.2320/MATERTRANS1960.12.147>.
- [35] J.O.S. Amistoso, A.V. Amorsolo, Thermal aging effects on Cu ball shear strength and Cu/Al intermetallic growth, *J. Electron. Mater.* 39 (2010) 2324–2331, <https://doi.org/10.1007/s11664-010-1320-3>.
- [36] C.S. Goh, W.L.E. Chong, T.K. Lee, C. Breach, Corrosion study and intermetallics formation in gold and copper wire bonding in microelectronics packaging, *Crystals* 3 (2013) 391–404. (<https://www.mdpi.com/2073-4352/3/3/391>).
- [37] S. Na, T. Hwang, J. Park, J. Kim, H. Yoo, and C. Lee, Characterization of intermetallic compound (IMC) growth in Cu wire ball bonding on Al pad metallization, 2011 IEEE 61st Electronic Components and Technology Conference (ECTC), pp. 1740–1745. <https://doi.org/10.1109/ECTC.2011.5898747>.
- [38] L. England and T. Jiang, Reliability of Cu Wire Bonding to Al Metallization, 2007 Proceedings 57th Electronic Components and Technology Conference, pp. 1604–1613. <https://doi.org/10.1109/ECTC.2007.374009>.
- [39] T. Wang, et al., Study on diffusion behavior and microstructural evolution of Al/Cu bimetal interface by synchrotron X-ray radiography, *J. Alloy. Compd.* 616 (2014) 550–555, <https://doi.org/10.1016/j.jallcom.2014.07.172>.
- [40] P. Xue, B. Xiao, Z.Y. Ma, Effect of interfacial microstructure evolution on mechanical properties and fracture behavior of friction stir-welded Al–Cu joints, *Metall. Mater. Trans. A* 46 (2015) 3091–3103, <https://doi.org/10.1007/s11661-015-2909-1>.
- [41] W.-B. Lee, K.-S. Bang, S.-B. Jung, Effects of intermetallic compound on the electrical and mechanical properties of friction welded Cu/Al bimetallic joints during annealing, *J. Alloy. Compd.* 390 (2005) 212–219, <https://doi.org/10.1016/j.jallcom.2004.07.057>.